Available online at www.sciencedirect.com

SciVerse ScienceDirect

Energy Procedia 34 (2013) 326 – 340

Energy Procedia

10th Eco-Energy and Materials Science and Engineering

(EMSES2012)

Speed and Power Control of a Slip Energy Recovery Drive Using Voltage-Source PWM Converter with Current Controlled Technique

Satean Tunyasrirut[a]*, Vijit Kinnares[b]

[a]*Department of Instrumentation and Control Engineering, Faculty of Engineering, Pathumwan Institute of Technology, 833 Rama 1 Rd. Pathumwan, Bangkok 10330, Thailand*
[b]*Department of Electrical Engineering, Faculty of Engineering, King Mongkut's Institute of Technology Ladkrabang, Chalongkrung Rd. Ladkrabang, Bangkok 10520, Thailand*

Abstract

This paper introduces the speed and power control a slip energy recovery drive using voltage-source PWM converter with current-controlled technique. The slip energy occurred in the rotor circuit is transferred back to ac mains supply through a reactor and a step up transformer. The objective of the current-controlled technique is to increase power factor of the system and to reduce low order harmonics of the input line current. The drive system is designed and implemented using a voltage source inverter in conjunction with a boost chopper for DC link voltage, instead of a conventional drive using a 6 pulse converter or a Scherbius system. The slip power is recovered by the help of a voltage source inverter (VSI) based on a current-controlled technique. In order to keep the speed of the wound rotor induction motor constant over a certain range of operating conditions, the servo state feedback controller designed by a linear quadratic regulator (LQR) is also introduced and the PI controller designed by pole placement method is also introduced in control the slip power this paper. The overall control system is implemented on DSP, DS1104'TMS320F240 controller board. A 1 kW wound motor is employed for testing. It is found that the motor speed can be controlled to be constant in the operating range of 600-1200 rpm at no load and full load. It is also found that the harmonics of the input ac line current is reduced while the ac line input power factor is increased.

Selection and peer-review under responsibility of COE of Sustainalble Energy System, Rajamangala University of Technology Thanyaburi (RMUTT)

Keywords: Slip energy recovery; wound rotor induction motor; voltage source inverter, current control ;

* *Corresponding author. Tel.: +662-104-9099 Exit8202; fax: +662-104-9098.*
E-mail address: satean2000@gmail.com

Selection and peer-review under responsibility of COE of Sustainalble Energy System, Rajamangala University of Technology Thanyaburi (RMUTT)
doi:10.1016/j.egypro.2013.06.761

1. Introduction

Induction motor drives with full power control on the stator side are commonly used in industrial applications. Although either a cage-type or wound rotor induction machine can be used in the drive, the former is always preferred in terms of low weight, low cost, low rotor inertia, speed limitation, maintenance and reliability. One feature of the latter is that the slip power becomes easily available from the slip rings, which can be either mechanically or electronically controlled for motor speed adjustment [1]. However, for limited range speed control applications, where the slip power is only a fraction of the total power rating of machine, power rating of the converter is reduced, hence reduction in cost. The wound rotor induction motor takes this advantage. Slip power for adjusting the motor speed can be recovered through static converters instead of useless dissipation on resistors. Slip power recovery drives have been used in some applications such as large-capacity pumps and fan drives, variable-speed wind energy systems, shipboard variable-speed/constant-frequency systems, variable-speed hydro pumps/generators and utility system flywheel energy storage systems. The slip energy recovery drives (SERD) known as Scherbius system [2-3], offer low cost, simple control circuitry and high efficiency even at a low speed range. The SERD consists of a wound-rotor induction machine, a diode-bridge rectifier, a large link inductance, a thyristor-bridge inverter and an optional 3 phase transformer. A SERD transfers power that is normally wasted in the rotor of an induction machine back to the ac mains supply to improve overall drive efficiency. In addition, by inserting a step-down transformer between the ac supply and the inverter module, the voltage ratings of the inverter and rectifier devices may be made significantly smaller than the rated machine stator voltages. Thus, in contrast with a stator-voltage-controlled induction machine drive, the relative power electronic units of the SERD may be designed to be smaller, lighter and less expensive. The choice of the turns-ratio of the optional transformer is based on a compromise between achieving the desired speed control range and optimizing the drive power factor [1]. For smaller values of inverter firing angle, the rotor speed is higher. Then inverter draws substantial reactive power and the inverter returns less real power to the mains. Thus the drive power factor is reduced. The drive power factor is found to be optimized for applications requiring a narrow range of speed control and a large load torque, where significant real power is returned via the inverter. A problem of SERD is having lower power factor in general 0.4 to 0.6 more or less. Drawbacks of SERD such as, 1) low power factor, 2) high current harmonic, and 3) a poor capability of the reactive power on the ac side, can be avoided by using a pulse width modulation (PWM) voltage source inverter. The drive system can control the active and reactive power on the ac line by a current-controlled technique in conjunction with the first and second a boost chopper for DC link voltage. The voltage source inverter is used to increase power factor of the system and to reduce low order harmonics of the input line current.

This paper presents a simple configuration that can completely solve the first and second problems and partially solve the third problem. Although there are a number of articles which analyze the SERD with dc voltage intermediate circuit. The system proposed in this paper differs from previously discussed approaches in the following ways. 1) There is a boost chopper on the intermediate circuit providing control of the machine. 2) A decoupled control system is achieved. Effectively, the machine speed is controlled by the boost chopper and the inverter controls the reactive power on the ac side. 3) The current harmonics on the mains are reduced by a VSI based on PWM [4-5].

The aim of this paper is two-fold. The first is that the harmonics of line current waveforms are reduced by using the VSI. The second aim is to improve the power factor of the drive by the IGBT type boost chopper applied across the DC terminal. The boost DC voltage is connected to the voltage source inverter and the reactor circuit. This scheme leads to be able to adjust the speed of the motor by varying the duty cycle of the boost chopper operating in a PWM mode.

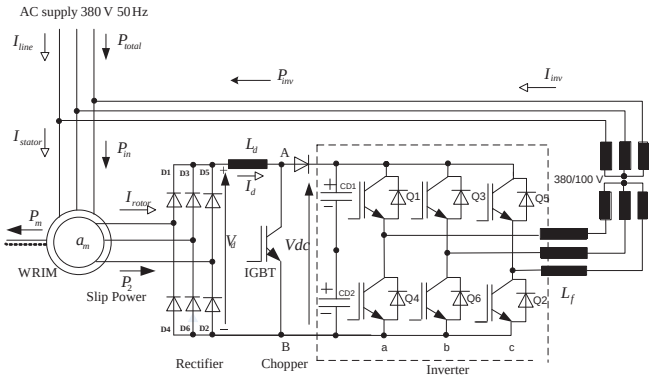

Fig. 1. Schematic of the proposed slip energy recovery drive with current controlled voltage source inverter

2. Current Controlled-Technique

The proposed system configuration is illustrated in Fig. 1. It's consists of an IGBT boost chopper, a diode D, a dc link capacitors and a PWM type VSI. The voltage, *Vdc* is controlled at a constant value by the IGBT boost chopper. Consequently variation of torque and speed is achieved by operation of the boost chopper.[4],[9-10] Using the diode bridge connecting the rotor of the machine to the electronic circuit allows a simplified control system. The active and reactive power can be controlled by controlling the current of voltage source inverter side and ac line side connected with the reactor circuits. An inductance L_d can be added on the dc side to decrease the switching frequency or the dc current ripple[2].

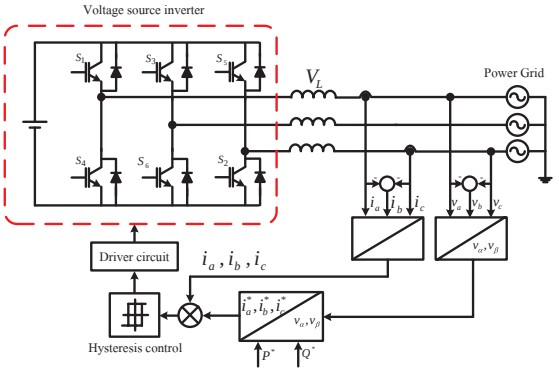

Fig. 2. Current Control Techniques for PWM Converter

From fig. 2 the grid voltage can be written to equation 1

$$v_{grid} = v_{conv} + v_L \tag{1}$$

The active and reactive power flow between grid side and converter side can be written to equation 2 and 3 [4-8]

$$P = \frac{V_{grid}^2}{\omega L}\left(\frac{V_{conv}}{V_{grid}}\sin\delta\right) \tag{2}$$

$$Q = \frac{V_{grid}^2}{\omega L}\left(1-\frac{V_{conv}}{V_{grid}}\cos\delta\right) \tag{3}$$

Where apparent power is

$$S = vi^* = P + jQ \tag{4}$$

The instantaneous real and imaginary power are part to the instantaneous complex power defined equation 5

$$S = \left(v_\alpha i_\alpha + v_\beta i_\beta\right) + j\left(v_\beta i_\alpha + v_\alpha i_\beta\right) \tag{5}$$

Where apparent power is

$$S = vi^* = P + jQ \tag{6}$$

The instantaneous real and imaginary power are part to the instantaneous complex power defined equation 7

$$S = \left(v_\alpha i_\alpha + v_\beta i_\beta\right) + j\left(v_\beta i_\alpha + v_\alpha i_\beta\right) \tag{7}$$

From the transformation matrixes, the Clark transformation and its inverse transformation become

$$\begin{bmatrix} v_\alpha \\ v_\beta \end{bmatrix} = \frac{2}{3}\begin{bmatrix} 1 & -\frac{1}{2} & -\frac{1}{2} \\ 0 & \frac{\sqrt{3}}{2} & -\frac{\sqrt{3}}{2} \end{bmatrix}\begin{bmatrix} v_a \\ v_b \\ v_c \end{bmatrix} \tag{8}$$

The instantaneous power of the $p-q$ theory

$$\begin{bmatrix} P \\ Q \end{bmatrix} = \begin{bmatrix} v_\alpha & v_\beta \\ -v_\beta & v_\alpha \end{bmatrix}\begin{bmatrix} i_\alpha \\ i_\beta \end{bmatrix} \tag{9}$$

In the following explanation, the $\alpha\beta$ currents will be set as functions of voltage and the real and imaginary power P and Q. This is very suitable for better explaining the physical meaning of the powers defined in the $p-q$ theory, it is possible to write

$$\begin{bmatrix} i_\alpha \\ i_\beta \end{bmatrix} = \frac{1}{v_\alpha^2 + v_\beta^2} \begin{bmatrix} v_\alpha & v_\beta \\ v_\beta & -v_\alpha \end{bmatrix} \begin{bmatrix} P \\ Q \end{bmatrix} \tag{10}$$

The inverse Clark transformation can be decomposed into the sum of two terms, as follows

$$\begin{bmatrix} i_a^* \\ i_b^* \\ i_c^* \end{bmatrix} = \frac{2}{3} \begin{bmatrix} 1 & 0 \\ -\frac{1}{2} & \frac{\sqrt{3}}{2} \\ -\frac{1}{2} & -\frac{\sqrt{3}}{2} \end{bmatrix} \begin{bmatrix} i_\alpha \\ i_\beta \end{bmatrix} \tag{11}$$

3. Modeling of DC Link

According to Fig. 3, the mathematical model of the system is analyzed by considering a simplified equivalent circuit of the dc link with the boost chopper [7],[12].

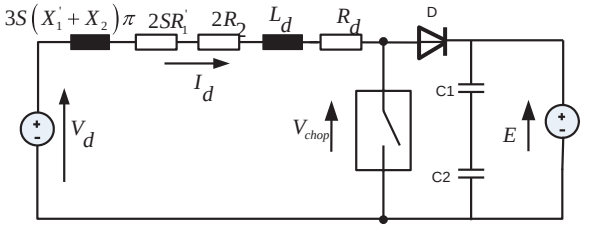

Fig.3. Circuit diagram of dc link.

Then the current in DC link can be determined from

$$\frac{di_d}{dt} = -\frac{1.35V_s}{L_d \omega_s} \omega_r - \frac{1}{\tau} i_d + \frac{1.35V_s}{a_m L_d} \left(1 - \frac{1}{1-D}\right) \tag{12}$$

Where a_m is the turns ratio of the stator to rotor. From Eq.(12), the speed of the motor can be controlled by changing the boost chopper voltage V_{chop} at the intermediate DC link by changing the duty cycle (D). Motor slip is given as

$$s = \frac{\omega_s - \omega_r}{\omega_s} \tag{13}$$

Equivalent electrical time constant can be defined as

$$\tau = \frac{L_d}{R_A + R_B} \tag{14}$$

Where $R_A = 2R_1^{'} + 3\left(X_1^{'} + X_2\right)/\pi$ and $R_B = 2R_2 + R_d$, $R_1^{'}$ is the stator resistance transferred to rotor side, $X_1^{'}$ is the stator leakage reactance transferred to the rotor side, X_2 is the rotor leakage reactance, R_2 is the rotor resistance and R_d is the resistance of the inductor.
The slip power for determining developed torque can be given as

$$P_2 = \frac{1.35sV_s}{a_m} i_d - \left(sR_A + R_B\right) i_d^2 \tag{15}$$

Electromagnetic torque can be given as

$$T_d = \frac{P_2}{s\omega_s} = \frac{1}{s\omega_s}\left(\frac{1.35sV_s}{a_m} i_d - \left(sR_A + R_B\right) i_d^2\right) \tag{16}$$

Neglecting copper loss in the dc link equivalent circuit, the second term of Eq.(17) can be omitted. Then,

$$T_d = \frac{1}{\omega_s}\left(\frac{1.35V_s}{a_m} i_d\right) \tag{17}$$

Torque equation neglecting friction is given as

$$T_m \frac{d\omega_r}{dt} = T_d - T_L \tag{18}$$

Where T_m is mechanical time constant. By considering load torque $T_L = 0$ and T_d from Eq.(18), then Eq.(19) can be rewritten as

$$\frac{d\omega_r}{dt} = \frac{1.35V_s}{a_m \omega_s T_m} i_d \tag{19}$$

The state space model takes the form:

$$\dot{\mathbf{x}} = A\mathbf{x} + Bu \tag{20}$$

$$y = C\mathbf{x} \tag{21}$$

To solve this model, first state variables must be assigned. Let $K_T = 1.35V_s / a_m\omega_s, K_a = \omega_s K_T / L_d$ and $u_a = \left(1 - \frac{1}{1-D}\right)$ Let the state variables $x_1 = \omega_r$, rotor angular speed and $x_2 = i_d$, dc link current. With the mentioned notation and from Eqs. (20) and (21), the system equations can be written in a matrix form as

$$\begin{bmatrix}\dot{x}_1\\ \dot{x}_2\end{bmatrix}=\begin{bmatrix}0 & \frac{K_T}{T_m}\\ -\frac{a_m K_T}{L_d} & -\frac{1}{\tau}\end{bmatrix}\begin{bmatrix}x_1\\ x_2\end{bmatrix}+\begin{bmatrix}0\\ K_a\end{bmatrix}u_a \tag{22}$$

$$y=\begin{bmatrix}1 & 0\end{bmatrix}\begin{bmatrix}x_1\\ x_2\end{bmatrix}. \tag{23}$$

In this work, the parameters of the system were tested with a plant model of the three phase wound rotor induction motor with the detail given in Appendix A. Then, resultant equation matrixes corresponding to Eqs. (20) and (21) which are referred to the general equations (22)and (23) can be achieved as follows

$$A=\begin{bmatrix}0 & 1.63\\ -2.17 & -16.7\end{bmatrix}, B=\begin{bmatrix}0\\ 17\end{bmatrix}, C=\begin{bmatrix}1 & 0\end{bmatrix}, D=0, u=u_a$$

$$y=\omega_r, x=\begin{bmatrix}x_1\\ x_2\end{bmatrix}=\begin{bmatrix}\omega_r\\ i_d\end{bmatrix}, \dot{x}=\begin{bmatrix}\dot{x}_1\\ \dot{x}_2\end{bmatrix}=\begin{bmatrix}\frac{d\omega_r}{dt}\\ \frac{di_d}{dt}\end{bmatrix}$$

4. Design of Controller

The speed control of motor is designed by Linear Quadratic Regulator, LQR using Matlab program. The servo state feedback controller designed is also introduced as shown in Fig.4. The system is completely state controllable.

$$u=-\begin{bmatrix}\mathbf{K} & -k_I\end{bmatrix}\begin{bmatrix}x\\ e\end{bmatrix} \tag{24}$$

The closed loop system can be written in state equations

$$\begin{bmatrix}\dot{\mathbf{x}}\\ \dot{\mathbf{e}}\end{bmatrix}=\begin{bmatrix}A-B\mathbf{K} & Bk_I\\ -C & 0\end{bmatrix}\begin{bmatrix}x\\ e\end{bmatrix}+\begin{bmatrix}0\\ 1\end{bmatrix}r \tag{25}$$

Where

$$\hat{A}=\begin{bmatrix}A & 0\\ -C & 0\end{bmatrix}=\begin{bmatrix}0 & 1.63 & 0\\ -2.17 & -16.7 & 0\\ -1 & 0 & 0\end{bmatrix}, \hat{B}=\begin{bmatrix}B\\ 0\end{bmatrix}=\begin{bmatrix}0\\ 17\\ 0\end{bmatrix} \text{ and } C=\begin{bmatrix}1 & 0 & 0\end{bmatrix}.$$

$$Q=\begin{bmatrix}100 & 0 & 0\\ 0 & 1 & 0\\ 0 & 0 & 1\end{bmatrix}, R=1$$

We can try to optimize [13]. To get a fast response, q_{11} must be sufficiently large compared with q_{22} and q_{33}. In this case, q_{11}, q_{22}, q_{33} and R were selected with 100, 1, 1 and 1 respectively. By using Matlab

command $[K,P,E]=lqr(A,B,Q,R)$, feedback matrix gain $\mathbf{K}$ resulting from this LQR design is $\mathbf{K}=[9.9 \quad 0.98 \quad -1]$.

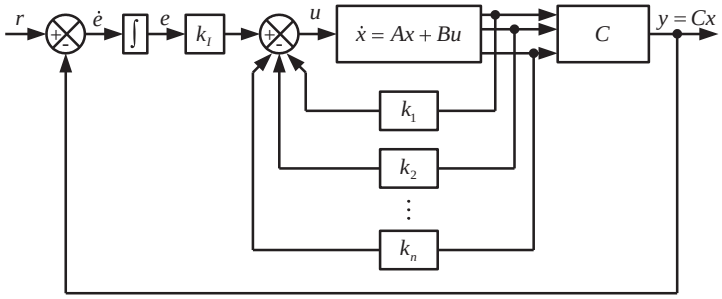

Fig. 4. Block diagram of servo state feedback controller.

5. Simulation Current Controlled-Technique

Current controlled-technique for voltage-source PWM converter applied for a slip energy recovery drive was simulated in the Matlab/Simulink software. The wound rotor induction motor is rated at 1 kW, 4 pole with a 380 V, 50Hz as shown in figure 5.

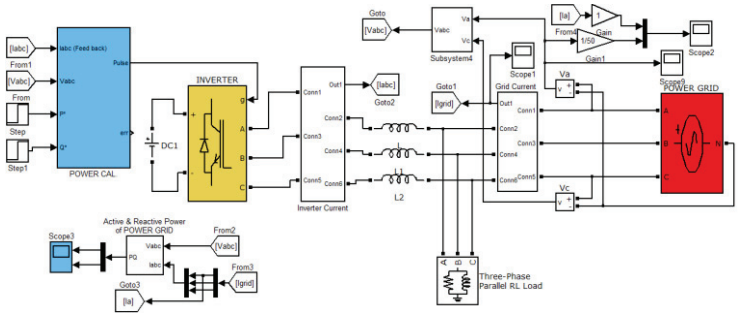

Fig. 5. Simulation of current controlled- technique for voltage-source PWM converter.

Fig.6 shows the simulated output phase voltage of converter (v_{ar}), the dc-link voltage (v_d), the supply phase voltage (v_{as}) and current (i_{as}) of the grid side converter operation at unity power factor, Q is set to zero, by the converter for operation in the rectifying mode. Fig. 7 also shows the voltage and the current waveforms of the converter operating in the inverting mode. As can be seen from Fig. 8, the dynamic response of the converter to a step changed in active power reference control with active power flowing from the supply in to the dc-link, rectifying mode. The setting of active power reference is stepped from -1000 watt to +1000 watt, it can be seen that the phase current of VSC can operate under the rectifying mode and inverting mode condition.

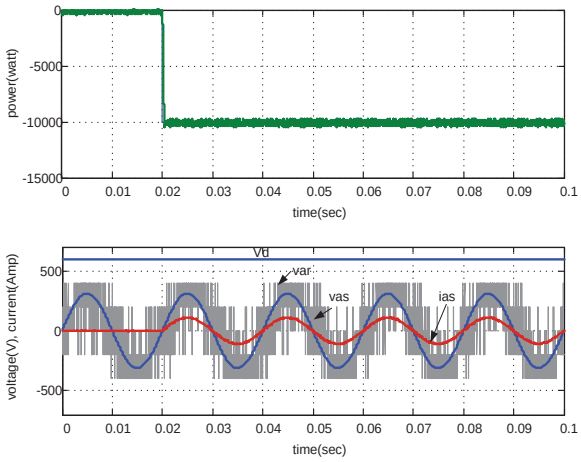

Fig. 6. Voltage and current waveforms, with the grid side converter working as a rectifying mode.

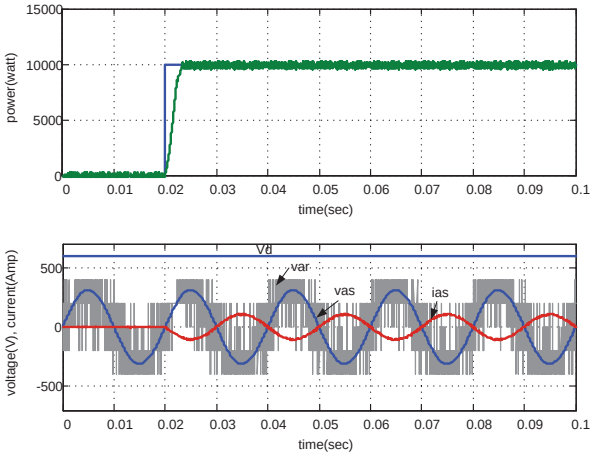

Fig. 7. Voltage and current waveforms, with the grid side converter working as a inverting mode.

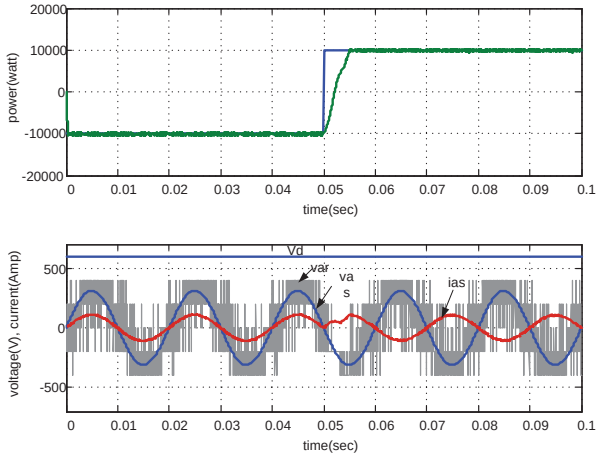

Fig. 8. Dynamic response of voltage and current operate under the rectifying mode and inverting mode condition.

6. Experimental Setup

The experimental setup as shown in Fig. 9, mainly consists of a dSPACE DS1104 DSP controller board, a Pentium IV 2.5 GHz PC with Windows XP, a four-pole wound rotor induction motor and the proposed voltage source inverter with the IGBT boost chopper. A 3600 pulse/rev incremental encoder for speed measurement is used. The DS1104 board is installed in Pentium IV PC. The control program is written in SIMULINK environment combined with the real-time interface of the DS1104 board. The main ingredient of the software used in the laboratory experiment is based on MATLAB/Simulink programs. The control law is designed in simulink and executed in real time using the dSPACE DS1104 DSP board. Once the controller has been built in Simulink block-set, machine codes are achieved that runs on the DS1104'TMS320F240 DSP processor. While the experimental is running, the dSPACE DS1104 provides a mechanism that allows the user to change controller parameter online. Thus, it is possible for the user to view the real process while the system is in progress. A dSPACE connector panel (CP1104) provides easy access to all input and output signals of the DS1104 board. The switching frequency of PWM for boost DC voltage the IGBT chopper is varied between 0-1500 Hz. The reason for using IGBT switching device is simplicity for control [14].

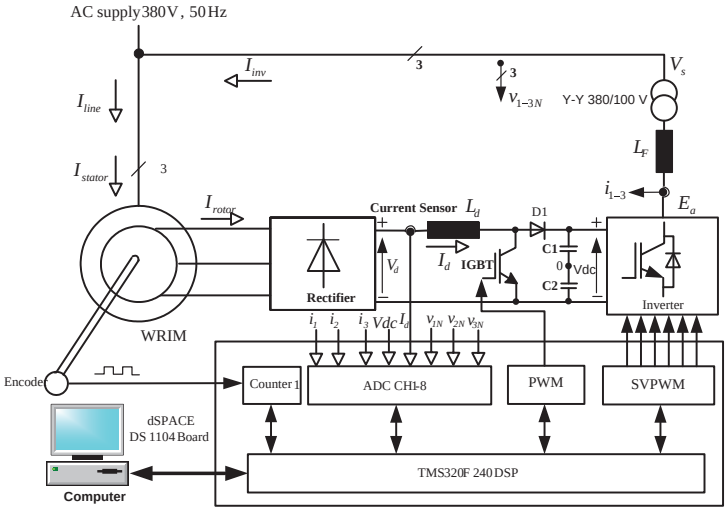

Fig. 9. Experimental setup.

7. Overall System Performance

The experimental performance results of the proposed drive are illustrated in case of:

(i) current waveforms and corresponding harmonics;
(ii) power quality of mains supply such as total harmonic distortion (THD), displacement power factor (DPF) and power factor (PF);
(iii) dynamic response.

7.1. The current waveforms and corresponding harmonic spectra of supply current

The phase voltage E_s, supply line current waveforms (I_{line}) and inverter current (I_{inv}) waveform results were measured by using LEM sensors. These waveforms were recorded by the digital power quality FLUKE 43B as shown in Figs. 10-11. In this figure show phase voltage E_s and supply line current and inverter current waveforms of the CC-VSI at slip 0.5 and at slip 0.2. These reveal that the current control voltage source inverter can help a reduction in fundamental current magnitude and an increase in power factor. Fig.12 show harmonic spectra of the supply line current corresponding. Trends of the magnitudes of the fundament current and harmonic contents of the proposed CC-VSI are reduced.

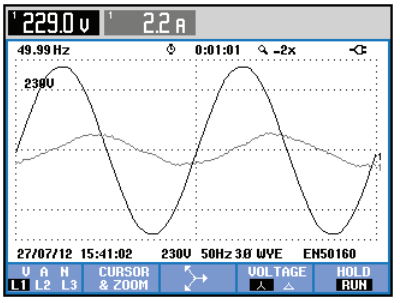

(a) at slip 0.5

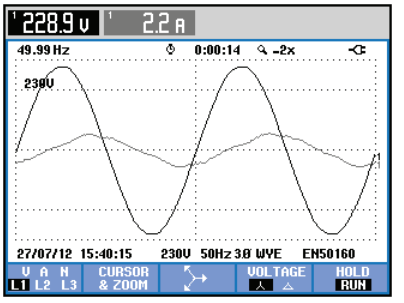

(b) at slip 0.2

Fig. 10. Phase voltage E_s and I_{line} waveforms.

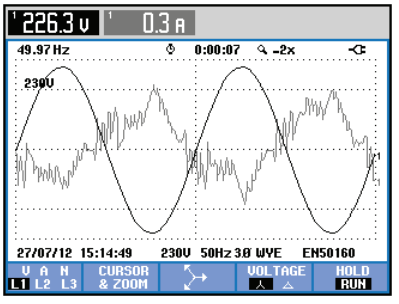

(a) at slip 0.5

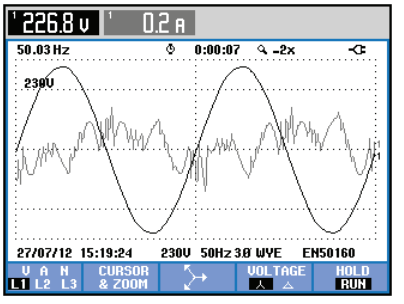

(b) at slip 0.2

Fig. 11. Phase voltage E_s and I_{inv} waveforms.

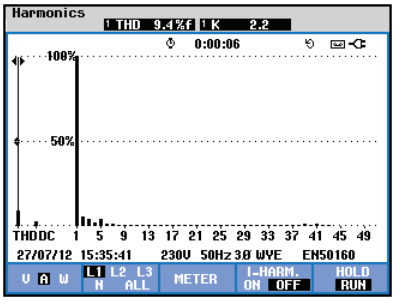

(a) at slip 0.5 (THDi=9.1%)

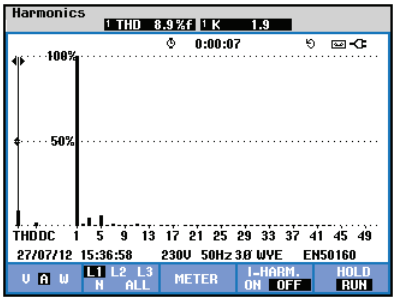

(b) at slip 0.2 THDi=8.6%)

Fig. 12. Harmonics spectrum of supply line current.

7.2. Power quality on mains supply and inverter side

The experimental results can be summarized as follows: The total harmonic distortion (THD), displacement power factor (DPF), power factor of ac mains supply and power were measured using the digital power quality FLUKE 43B at 100% load torque. Figs. 13-14 show drive performance at slip of 0.5 and 0.2(near rated speed operation) respectively. The proposed CC-VSI gives high power factor and displacement power factor. Power factor, displacement power factor and efficiency for all drives at high speed operation are higher than at low speed operation. These agree with the characteristic of the conventional Scherbius system as mentioned before. It is noted that generally slip power recovery drives give quite low efficiency particularly at a low speed region. Total harmonic distortion of the supply current for the proposed CC-VSI is much better than conventional SRED at low to high speed operation. These results confirm the performance improvement and the increase in overall system efficiency for the proposed drive.

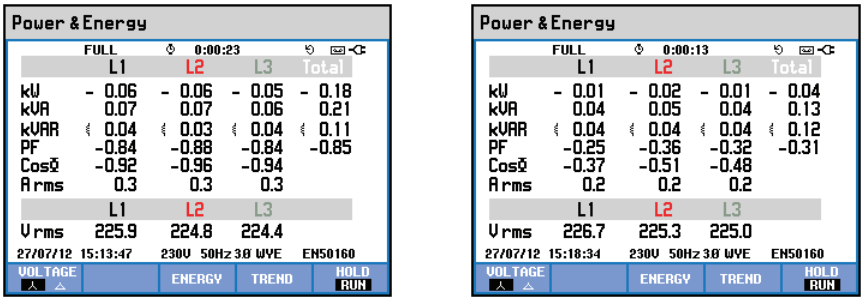

(a) at slip 0.5 (b) at slip 0.2

Fig. 13. Power quality on inverter supply

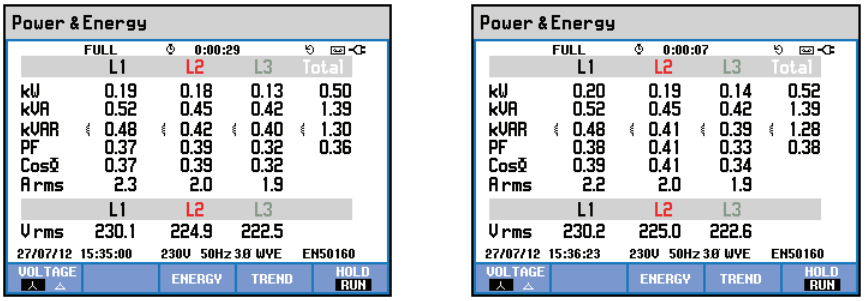

(a) at slip 0.5 (b) at slip 0.2

Fig.14.Power quality on mains supply.

7.3. Response of Speed

To evaluate the performance of the system, a series of measurements has been conducted. The measurements can be divided in two groups: the first is a step change of the speed reference at constant load torque and the second is a step change of the load torque at constant speed reference. As shown in Figs. 15-16 at a servo state feedback gain $k_1 = 9.9$, $k_2 = 0.98$ and $k_I = -1$, time response of speed is tested by the step change of speed reference 750 to 1200 rpm with the load torque of zero and rated values respectively. It has been found that the rise time $t_r = 0.5\,\text{s}$, peak time $t_p = 1\,\text{s}$, settling time $t_s = 2\,\text{s}$,

maximum overshoot $MP = 17$ %. Responses for a step change of the load torque at constant speed reference are shown in Figs. 17-18. The settling time t_s is within 1 s.

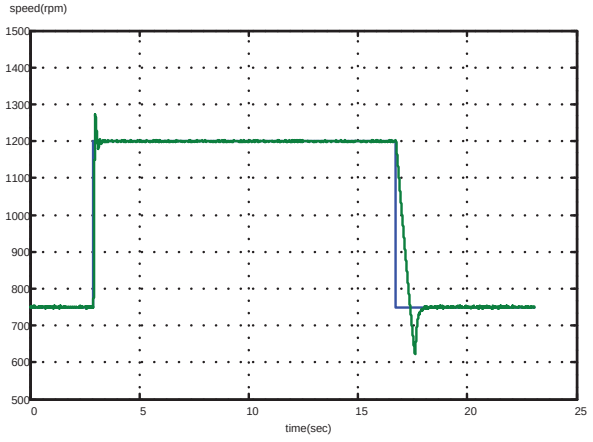

Fig. 15. Step change of speed reference 750-1200 rpm at zero load.

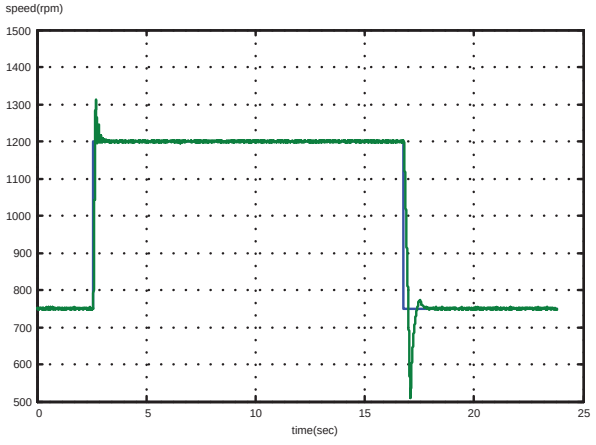

Fig. 16. Step change of speed reference 750-1200 rpm at rated load.

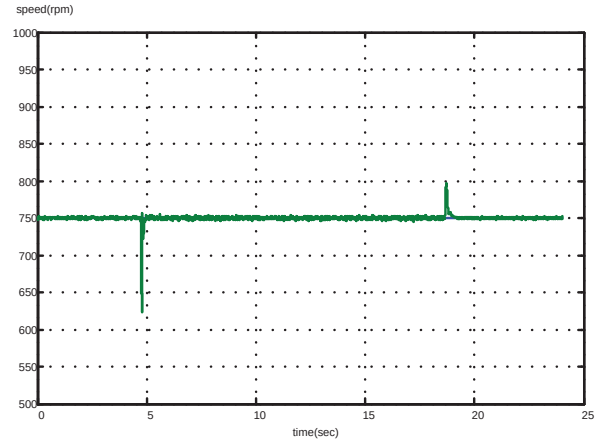

Fig. 17. Step change of load torque at constant speed reference 750 rpm.

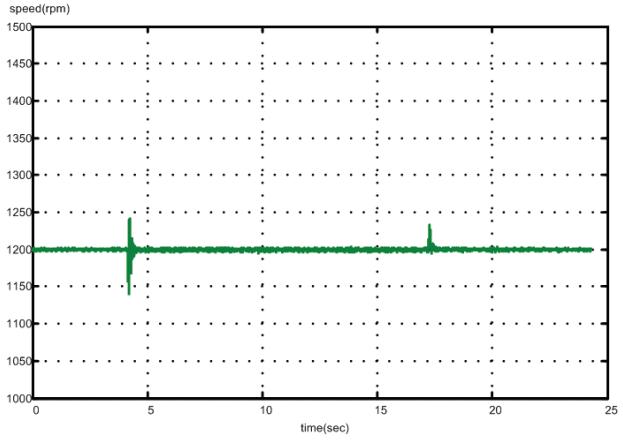

Fig. 18. Step change of load torque at constant speed reference 1200 rpm.

8. Conclusion

In this paper, the current control technique for voltage-source PWM converter applied for a slip energy recovery drive can be achieved. The total harmonic distortion of the supply line current waveforms are reduced to 9.1 % at slip 0.5 and 8.6 % at slip 0.2 respectively. The power factor obtained from CC-VSI with a boost chopper for DC link voltage is at inverter side have been 0.85 at slip 0.5 and 0.31 at slip 0.2 respectively. The servo state feedback controller is applied to speed signal model of the motor and is then downloaded to dSPACE board DS1104 through Simulink. The experimental results testing with the 1000 watt wound rotor induction motor at zero load condition to rated condition have shown obviously the performance improvement. It has been found that the speed of the induction motor can be controlled at the desired speed. In addition, the motor speed can keep constant when the load varies. Due to the control of motor speed, active and reactive power with either the adjustment of the duty cycle of a chopper or the adjustment of the hysteresis of a CC-VSI, this technique also offers an advantage in ease of control. In addition, with a small size of a converter to handle slip power about 30% of rated machine power, certainly, it can be applied to the full scale practice particularly for high power pump and renewable applications.

Acknowledgements

The work presented in this paper has been supported financially by the Thailand Research Fund, Office of the Higher Education Commission and Pathumwan Institute of Technology, Bangkok, Thailand.

References

[1] Bose, Bimal K, Modern power electronics and ac drives, ©2002 Prentice Hall PTR, Prentice-Hall, Inc, pp. 307-331.

[2] W. Leonharn, Control of electrical drives, Springer-Verlag Berlin Heidelberg, New York, Tokyo, 1985, pp. 245-259.

[3] R. Krishnan, Electric motor drives modeling analysis and control, ©2001 Prentice Hall , Prentice-Hall, Inc, pp. 282-308.

[4] C. Picardi and D. Sgro. "Grid-Connected Inverter Power Flow Control Based on a New Modeling Approach of Electrical Signal" IEEE International Conference. PP 585-590, 2009.

[5] N. Mohand, T. M. Undeland and W. P. Robbins, "Power Electronics: Converters, Applications, and Design", John Wiley & Sons, 3rd edition, 2003.N. Mohand. T

[6] G. H. Bode and D. G. Holmes "Implementation of Three Level Hysteresis Current Control for a Single Phase Voltage Source Inverter", Power Electronics Specialists Conference, PP. 33-38, Vol. 1, 2000.

[7] N. Mohand, T. M. Undeland and W. P. Robbins, "Power Electronics: Converters, Applications, and Design", John Wiley & Sons, 3rd edition, 2003.

[8] H.Akagi, E. H. Watanabe and M. Aredes, "Instantaneous Power Theory and Applications to Power Conditioning" IEEE Press, John Wiley & Sons, 2007.

[9] M. P. Kazmierkowski and L. Malesani, "Current Control Techniques for Three-Phase Voltage-Source PWM Converters : A Survey" IEEE Transaction on Industrial Electronics, Vol. 45, No. 5, 1998.

[10] Hadi Saadat, Power System Analysis, Basic Principles Complex Power, The McGraw-Hill Companies, 1999.

[11] Yasuhiko Dote, Application of Modern Control Techniques to Motor Control, 018-9219/88/0400-0438/$01.00 ©1988 IEEE, pp. 438-453.

[12] S.A. Papathanassiou and M.P. Papadopoulos, State-Space Modeling and Eigenvalue Analysis of the Slip Energy Recovery Drive, IEE Proc-Electr. Power Appl. Vol. 144, No. 1, January 1997, pp. 27-36.

[13] K. Ogata, Modern Control Engineering, 4th ed., Prentice Hall International,2002, pp. 855–910.

[14] University of Minnesota, Introduction getting started with dSPACE, DSP based laboratory of electric drives.

Appendix A. Motor data and system parameters

Rated power	1 kW
Frequency	50 Hz
Rated speed	1420 rpm
Input voltage Δ/Y	230/400 V
Rotor voltage	100 V
Input current Δ/Y	4.8/2.8 A
Rotor current	7.6 A
Power Factor	0.71
Turn ratio of motor winding	4
Large Link Inductor (L_d)	750 mH
Electrical Time constant (τ)	60 ms
Mechanical Time constant (T_m)	250 ms
Total resistance DC link circuit $(R_A + R_B)$	12.5 Ω